1D-3D coupling investigation of hydraulic transient for power-supply failure of centrifugal pump-pipe system

Xiaoqin Li, Xuelin Tang, Min Zhu and Xiaoyan Shi

ABSTRACT

In the pumping station, the main feedwater system and the reactor system of nuclear power plant, power-supply failure causes strong hydraulic transients. One-dimensional method of characteristics (1D-MOC) is used to calculate the transient process in the pipeline system while three-dimensional (3D) computational fluid dynamics is employed to analyze the turbulent flows inside the pump and to obtain the performance parameters of the pump, and the data exchanges on the boundary conditions of the shared interface between 1D and 3D domains are updated based on the MpCCI platform. Based on the equation of motion of the pump motion parts, the relationship between the external characteristics and the internal flow field in the pump is further investigated because the dynamic behavior of the pump and the detailed fluid field evolutions inside the pump are captured during the transition process, and the transient flow rate, rotating speed, and pressure inside the impeller are comprehensively investigated. Meanwhile, compared with the data gained by experiment and traditional 1D-MOC, the relative errors of rotating speed and the flow rate obtained by 1D-3D coupling method are smaller than those by 1D-MOC. Furthermore, the influences of the main coupling parameters and coupling modes on the calculation results are analyzed, and the cause of the deviation is further explained.

Key words | 1D-3D coupling, hydraulic system, power-supply failure, transient, water hammer

Xiaoqin Li (corresponding author)
Xuelin Tang
Xiaoyan Shi
Beijing Engineering Research Center of Safety and Energy Saving Technology for Water Supply Network System,
China Agricultural University,
Beijing 100083,
China
E-mail: *mlp84238@163.com*

Min Zhu
Laibin Industry and Information Technology Commission,
Laibin, 546100,
China

INTRODUCTION

In recent years, more and more water supplies, irrigation and drainage projects, main feedwater systems and reactor systems in nuclear power plants have been built. In these hydraulic systems, the pipe flow changes caused by sudden power-supply failure can lead to water hammer pressure to the pipelines and hydraulic machinery, which could induce a strong impact on flow components such as pipeline, surge tank, valve and pump, and the pipe will even vibrate strongly or sometimes break under the condition of large pressure fluctuation. At the same time, the backflow and reversal of the pump will cause potential danger to the system (Cui *et al.* 2017).

A one-dimensional (1D) method of characteristics (MOC) (Wylie & Streeter 1993; Kiyama *et al.* 2016) is used to calculate the transition process including the changes of the flow rate, the pressure in the pipeline system and the rotating speed of the unit for the hydraulic system because its high calculation efficiency is suitable for dealing with various complicated boundary conditions and long pipeline systems. At present, most transition processes for hydraulic systems are studied by 1D-MOC. Hwang *et al.* (2012) developed a novel particle method of characteristics to simulate unsteady pipe flows and the method was used to solve some problems with significant transient effects in a single pipe flow. Nerella & Rathnam (2015) demonstrated the bench mark problem in a hydraulic system with a reservoir on the upstream end and a valve downstream of the pipeline end, and then obtained fluid pressure and flow rate variations in the pipeline with respect to time after the valve closure from the MOC model for one pipe system. Wang

doi: 10.2166/hydro.2019.122

& Yang (2015) combined the MOC and the implicit method to simulate pipeline unsteady flow under transient processes in a hydropower station, and applied the coupling method to determine the water-level fluctuation in the surge tank in one station and to solve the water hammer changing in a variable-area draft for a pump-turbine hydraulic system in another station. Meniconi *et al.* (2014) studied unsteady friction in detail and built an expression for the head envelope damping for turbulent flows in smooth and rough pipes. However, the computational accuracy of 1D-MOC is constrained because the static complete characteristic curve of the similar specific speed pump, instead of its dynamic characteristic curve, is often used to calculate the transient process due to the limits of the complete characteristic curve (Freni *et al.* 2013; Acosta *et al.* 2015). Meanwhile, it is difficult to describe the transient characteristic of the complex components for a three-dimensional (3D) hydraulic system by using 1D-MOC.

The 3D computational fluid dynamics (CFD) technology is mainly applied to analyze the internal flow for the hydraulic machinery due to its high computational accuracy (Liu *et al.* 2013; Hooff *et al.* 2017) providing plenty of flow-field information. Zou *et al.* (2016) analyzed the relationship between the evolution of transient radial force and the varying axial-to-spiral vortex structure during the start-up process of a large double suction centrifugal pump using CFD. Zhao & Zhao (2018) simulated the 3D transient internal flow of a centrifugal pump based on SST k-ω turbulence model combined with a homogeneous equilibrium model and obtained the effects of the diameter size and the concentration of particles on the flow field, the external performance, velocity, pressure, turbulent kinetic energy distribution and peak amplitude of pulsation frequency. Kong *et al.* (2015) studied the starting transient flows of a supersonic vacuum ejector-diffuser system with a newly designed chevron lobe and its performance characteristics, analyzed the equilibrium flow behavior inside the secondary chamber by using RNG k-ω model, and discussed simultaneously the generation process of the longitudinal vortexes and its effects on the ejector-diffuser performance. Martins *et al.* (2016, 2018) developed a CFD model corresponding to the best compromise between the maximum accuracy and the minimum computational effort to analyze the flow dynamics in pressurized pipes during the hydraulic transient process, and defined the most efficient set of discretization parameters capable of capturing the main features of the examined transient. Meanwhile, the energy dissipation phenomena during transients with low Reynolds number is discussed (Martins *et al.* 2017). However, the 3D-CFD technology makes it very hard to realize the 3D simulation for the whole pipeline system in the transient process because of the restricted computational time, computer resources, and computing stability. Therefore, it is only employed for some important parts of the system such as the impeller, valve, volute, and draft tube.

In recent years, 1D and 3D multi-scale numerical techniques have been coupled to calculate the transient process for pipeline systems. Many scholars have carried out corresponding applications and research (Grunloh & Manera 2016). Watanabe *et al.* (2006) developed an approach to achieve the data exchange on the interface between 1D and 3D, and this methodology was validated in calculating the internal flow inside a water circuit for an engine cooling system. Pei *et al.* (2013) investigated the characteristics of transient flow driven by all the rotating components in a single-blade sewage centrifugal pump based on the two-way coupling method. Panov *et al.* (2014) proposed an approach to simulate the unsteady cavitating flow in the flow passage for a hydraulic power plant, in which 1D hydro-acoustics equations were solved for the penstock domain, 3D equations of turbulent flow of isothermal compressible liquid-vapor mixture were solved for the turbine domain and cavitation was described by a transfer equation for liquid phase with a source term. Zhang *et al.* (2014) adopted the coupling analysis method considering the compressibility of water to calculate the transient internal flow of a turbine during the load rejection transition process, and it was concluded that the difference between the coupling calculation and 1D calculation was small, but the internal flow mechanism of the two methods was completely different. Wang *et al.* (2017) proposed a new coupling approach between the 1D-MOC and the 3D finite volume method of CFD, and applied it to the transient compressible flow caused by the closing and opening of a knife valve in a pipe system, in which the MOC code was implemented as boundary conditions in the OpenFOAM CFD source software and the coupling was realized by two linear equations originating from the characteristics equation and the Riemann constant equation. Zhou *et al.*

(2017) developed a 1D-3D coupling methodology to investigate the instantaneous flow characteristics of the residual heat removal pumps (RHRPs) system during the start-up process, in which the 1D flow in the pipe system was calculated by Euler equations and the SST k-ω turbulence model was applied to calculate the 3D flow field in the RHRPs.

Although more and more scholars have focused on the superiority of the coupling calculation, the coupling method for calculating and analyzing the power-supply failure process is rarely reported. The coupling solution method and coupling parameters have a great influence on the calculation results, but those are seldom studied. Therefore, in this paper the 1D-3D coupling method was used to simulate the transition process for a pump hydraulic system during power-supply failure in order to obtain the 1D transient characteristics of the pipeline system and the 3D internal flow of the centrifugal pump.

1D-3D COUPLING METHOD IMPROVEMENT

1D-MOC

1D-MOC is one of the most common methods to analyze the water hammer caused by a change of flow in the pipe system (Wylie & Streeter 1993). The commercial Flowmaster software is based on this method for transient process calculation. The water hammer governing equations include a momentum equation and continuity equation, which can be transformed into two partial differential equations as follows:

$$v\frac{\partial H}{\partial x}+\frac{\partial H}{\partial t}+\frac{a^2}{g}\frac{\partial v}{\partial x}+v\sin\alpha=0 \tag{1}$$

$$\frac{\partial v}{\partial t}+v\frac{\partial v}{\partial x}+g\frac{\partial H}{\partial x}+\frac{fv}{2d}|v|=0 \tag{2}$$

where H is the water head of the piezometer; v is the flow velocity; a is the water wave velocity in the pipe; g is the gravitational acceleration; f is the pipe friction coefficient; d is the pipe diameter; α is the pipe inclination angle; x is the distance along the pipe; t is the time.

In Equation (2), the friction term has an influence on the calculation results. Constant friction and unsteady friction are commonly used. Unsteady friction is dealt with by using a quasi-two-dimensional method, convolution integral method and instantaneous acceleration method. The constant friction is good for approximating the first peak value of unsteady pressure, and the error is small when determining the maximum or minimum pressure for single operating conditions, but there are probably some relative errors of the calculation for multiple operating conditions detailed in the literature (Chaudhry 2014). Therefore, constant friction is adopted because the transient process for the case discussed in this paper is for a single operation as opposed to multiple operations.

Equations (1) and (2) are the basic equations for 1D pipe systems under unsteady conditions. The equations are hyperbolic partial differential equations and can be solved by different methods, in which the elasticity is not fully considered. The equations are solved by applying the MOC because it can be used to deal with the complex boundary conditions and its calculations in each boundary and each pipe section are independent at each time step.

Method of 3D flow simulation

The governing equations for the turbulent incompressible flow are presented in the following forms.

Mass conservation equation:

$$\frac{\partial \rho}{\partial t}+\frac{\partial(\rho u_i)}{\partial x_i}=0 \quad i=1,2,3 \tag{3}$$

Momentum conservation equation:

$$\frac{\partial}{\partial t}(\rho u_i)+\frac{\partial(\rho u_i u_j)}{\partial x_j}=-\frac{\partial p}{\partial x_i}+\frac{\partial}{\partial x_j}\left[\mu\left(\frac{\partial u_i}{\partial x_j}+\frac{\partial u_j}{\partial x_i}\right)\right]+G_i \tag{4}$$

where ρ is the density; p is the transient pressure; μ is the molecular viscosity; x_i and x_j are the different coordinate components, u_i and u_j are the components of the flow velocity in each direction; and G_i is the volume force.

The flow in the double suction centrifugal pump is relatively complicated during the transient process owing to flow separation. The RNG k-ε two-equation model is applied to calculate the internal flow field because the model has a good computational precision suitable for the rotating flow (Koufi *et al.* 2017). The transport equations of

the RNG k-ε model for the simulation are as follows:

$$\frac{\partial(\rho k)}{\partial t}+\frac{\partial(\rho k u_i)}{\partial x_i}=\frac{\partial}{\partial x_j}\left[\alpha_k \mu_{eff}\frac{\partial k}{\partial x_j}\right]+P_k+\rho\varepsilon \tag{5}$$

$$\frac{\partial(\rho \varepsilon)}{\partial t}+\frac{\partial(\rho \varepsilon u_i)}{\partial x_i}=\frac{\partial}{\partial x_j}\left[\alpha_\varepsilon \mu_{eff}\frac{\partial \varepsilon}{\partial x_j}\right]+\frac{\varepsilon}{k}(C_{1\varepsilon}{*}P_k-C_{2\varepsilon}\rho\varepsilon) \tag{6}$$

where k is a turbulent kinetic energy; ε is the dissipation rate per unit volume; P_k is the turbulent kinetic energy generation term as follows:

$$P_k=\mu_t\left(\frac{\partial \mu_i}{\partial x_j}+\frac{\partial \mu_j}{\partial x_i}\right)\frac{\partial \mu_i}{\partial x_j} \tag{7}$$

$\mu_{eff}=\mu+\mu_t$ is the equivalent viscosity coefficient; $C_{1\varepsilon}^*$ is the coefficient as follows:

$$C_{1\varepsilon}^*=C_{1\varepsilon}-\frac{\eta(1-(\eta/\eta_0))}{1+\beta\eta^3} \tag{8}$$

$$\begin{cases}\eta=(2E_{ij}\cdot E_{ij})^{1/2}\dfrac{k}{\varepsilon}\\ E_{ij}=\dfrac{1}{2}\left(\dfrac{\partial \mu_i}{\partial x_j}+\dfrac{\partial \mu_j}{\partial x_i}\right)\end{cases} \tag{9}$$

μ_t is the eddy viscosity, which is expressed by Equation (10) for high Reynolds number flow and by Equation (11) for low Reynolds number flow, respectively:

$$\mu_t=\rho C_\mu\frac{k^2}{\varepsilon} \tag{10}$$

$$\begin{cases}d\left(\dfrac{\rho k^2}{\sqrt{\varepsilon\mu}}\right)=1.72\dfrac{\hat{\mu}}{\sqrt{\hat{\mu}^3-1+C_V}}d\hat{\mu}\\ \hat{\mu}=\dfrac{\mu+\mu_t}{\mu}\end{cases} \tag{11}$$

The above model constants are given as follows:

$$C_{1\varepsilon}=1.42,\ C_{2\varepsilon}=1.68,\ C_\mu=0.0845,\ \alpha_k=\alpha_\varepsilon=1.39,\ \eta_0=4.377,\ \beta=0.012,\ C_V\approx 100 \tag{12}$$

Platform of 1D-3D coupling

The coupling platform of MpCCI is used to exchange the data between 1D and 3D calculations in this paper. Data transmission includes two directions: one is from an upstream reservoir to the pump inlet and the other is from the pump outlet to the downstream reservoir as shown in Figure 1. Commercial Flowmaster software is used for 1D simulation of the pipeline system and Fluent software is adopted for 3D simulation of the centrifugal pump. The inlet and outlet of the pump are set as the coupling interfaces during the transient calculation. First, the MpCCI calls the Fluent module and sends the flow rate obtained from the Flowmaster software to the Fluent at the pump inlet coupling interface as the inlet boundary condition, while the pressure obtained from the Flowmaster software is transferred to the Fluent software at the pump outlet coupling interface as the outlet boundary condition, and then the internal flow field of centrifugal pump is calculated by the Fluent software. At the end of CFD completion at one step, the Fluent software passes the calculated pressure to the Flowmaster software at the inlet coupling interface and the calculated flow rate to the Flowmaster software at the outlet coupling interface, and then the transient process is calculated by Flowmaster. The abovementioned cycle is performed until the end of computation convergence, and

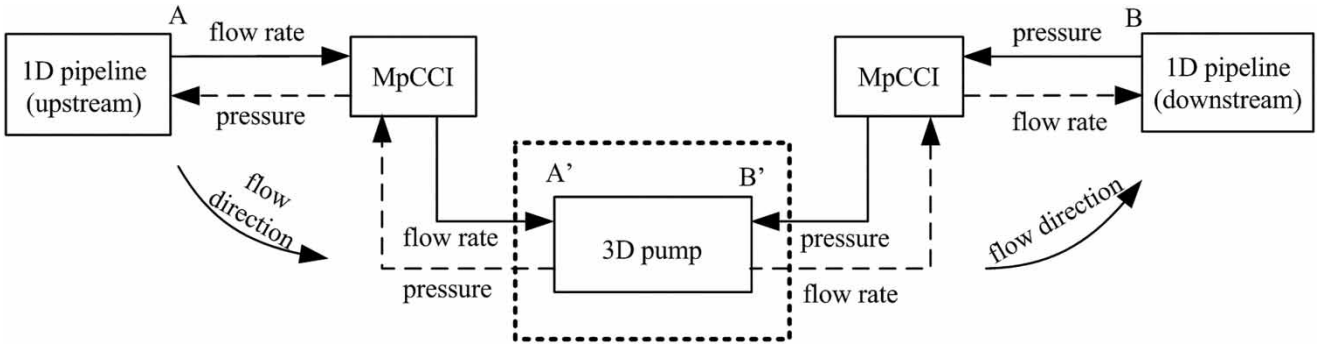

Figure 1 | Schematic diagram of coupling data transmission.

the transient parameters are obtained by using a coupling calculation.

INVESTIGATION SCHEME ON 1D-3D COUPLING OF CENTRIFUGAL PUMP-PIPE SYSTEM

Centrifugal pump-pipe hydraulic system

The centrifugal pump-pipe hydraulic system consists of an upstream reservoir, inlet pipe, double suction centrifugal pump, valve, outlet pipe and downstream reservoir as shown in Figure 2. The 3D calculation model of the centrifugal pump is established by using the Fluent software, and the 1D calculation model of the pipeline is carried out by using the Flowmaster software, which are shown in Figure 3.

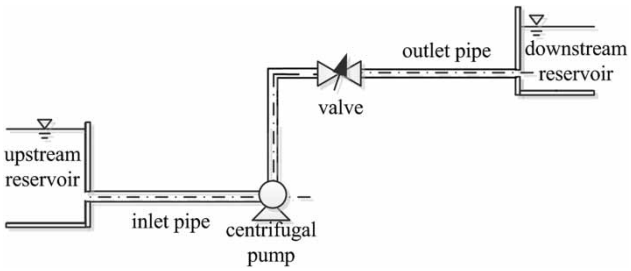

Figure 2 | Schematic layout of centrifugal pump-line hydraulic system.

The main parameters of the double suction centrifugal pump unit are as follows: the rated flow rate is 80 m^3/h, the rated head is 15 m, the rated rotating speed is 2,950 r/min, the blade number is 6, the specific speed is $n_s = 3.65n\sqrt{Q/2}H^{3/4} = 148.91$, the inlet diameter of the pump is 100 mm, the outlet diameter of the pump is 80 mm, and the diameter of the impeller is 130 mm. The suction-pipe length is 6 m and the discharge-pipe length is 24 m. The inertia moment of the pump is 0.01 kg·m^2 and the inertia moment of the motor is 0.115 kg·m^2. The 3D model of the centrifugal pump is demonstrated in Figure 4.

3D calculation schemes

The computational domain of the double suction centrifugal pump is meshed by ICEM software. The block grids are adopted to improve the grids' quality and to reduce the number of grids. The structural grids are applied for the blocks with simple structures and regular shapes (volute and extension sections at the inlet and the outlet, respectively), and the unstructured grids are used for the other complex shape parts including the impeller and suction

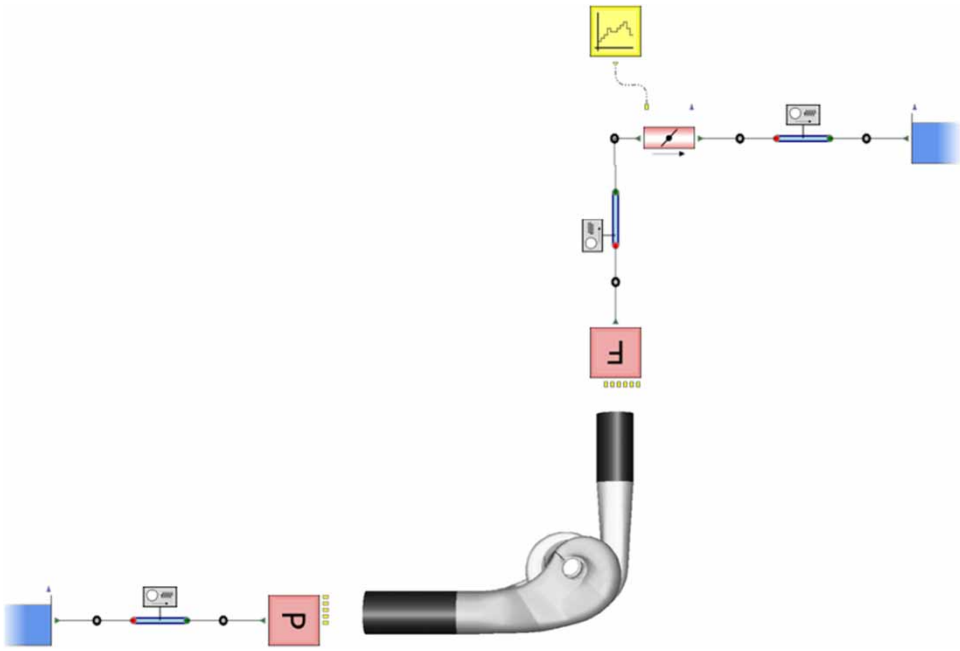

Figure 3 | Centrifugal pump-line system coupling calculation diagram.

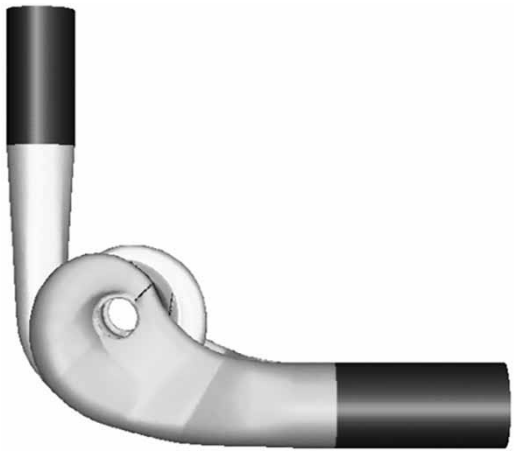

Figure 4 | 3D model of double suction centrifugal pump.

chamber, while the grid numbers are added near the blade leading edge, the blade tailing edge and the volute tongues, and the grids near the wall are also dense for obtaining the boundary layer flow to accurately calculate the shear force near the wall boundary. The grids of volute, suction chamber and impeller are shown in Figure 5.

For CFD computations, the wall boundary is the non-slip condition. The inlet and the outlet boundary conditions are provided by Flowmaster software, the boundary conditions at the inlet and the outlet are the mass flow rate and pressure, respectively. The RNG k-ε turbulence model is employed to solve the conservation equations of the mass and momentum. The second order upwind scheme is used for the convection term, the central difference scheme is adopted for the diffusion term and the second order implicit formula is selected for the time-dependent term. The RNG k-ε model is suitable for high Reynolds numbers, but the flow Reynolds number near the wall area is low. Therefore, the non-slip boundary condition combined with the standard wall function is applied to solve the flow near the wall area. The SIMPLE algorithm is used for the velocity-pressure coupling. The residual convergence precision is set to 0.0001.

In this paper, three grid schemes are selected for numerical simulation under rated operating conditions. The RNG k-ε model is adopted, and the convergence accuracy is 10^{-3}. The total grid numbers of the three schemes are

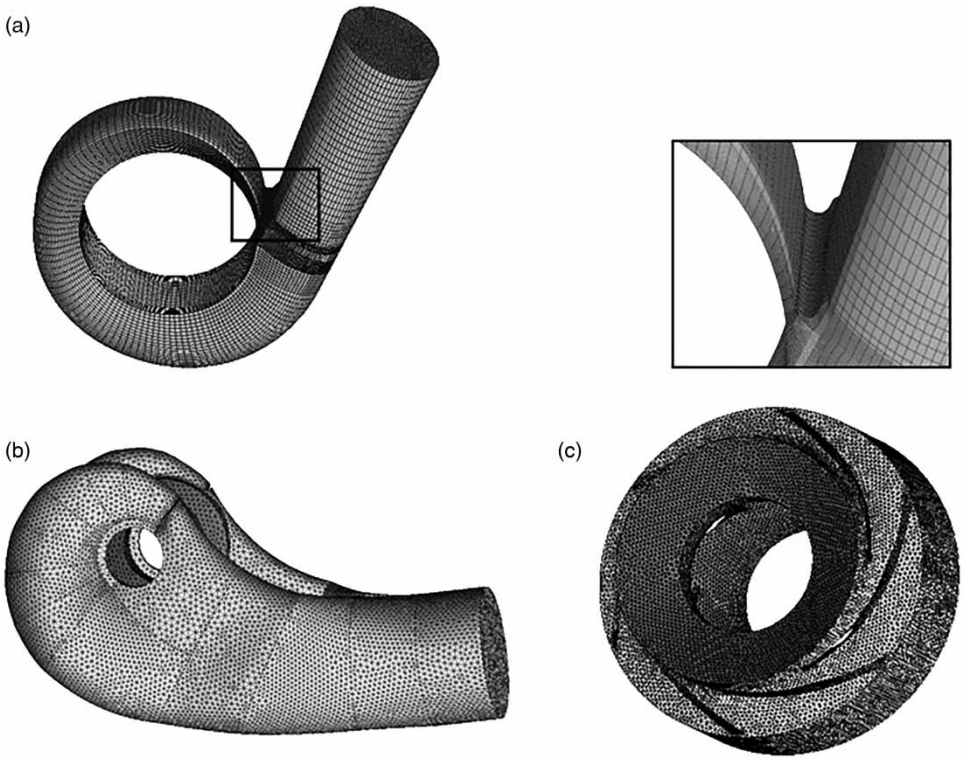

Figure 5 | Grids of volute, suction chamber and impeller. (a) Volute, (b) suction chamber, (c) impeller.

1.914×10^6, 2.647×10^6 and 4.451×10^6, respectively, to validate the grid-independent trial. The calculated water head, flow rate and efficiency are shown in Table 1. Both the calculated results by scheme B and those by scheme C are closer to the experimental value. When Flowmaster, Fluent and MPCI are coupled, memories will be occupied. Therefore, considering the computational efficiency, scheme B is selected for the coupling calculation to simultaneously meet the computational requirements and calculation error.

Data exchange schemes on coupling calculation method

In the coupling calculation, Fluent CFD software is used as the main calculation program for the internal flow of the pump. After the initial calculation, the data of flow rate and the pressure is transmitted to Flowmaster for the first coupling calculation based on the MpCCI platform. In addition, the time step of the coupling calculation is set according to the calculation requirements of 1D and 3D. The MpCCI provides a subcycling method for a smaller time step in 3D calculating for the Fluent software, which performs a CFD process by using a smaller time step in a coupling step, and then transfers the CFD data to the Flowmaster software. A data exchange diagram is shown in Figure 6, where Δt represents the time step, the solid line expresses the calculation process, and the dotted line is the data transfer process.

Table 1 | Grid-independent trial

Scheme	A	B	C	Experimental value
Grid number/10^6	1.914	2.647	4.451	–
Water head/m	16.5	15.91	15.59	15.08
Efficiency/%	80.07	79.80	80.11	69.85

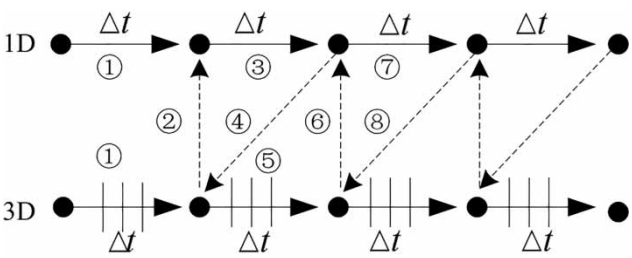

Figure 6 | Schematic diagram of data transfer.

The initialization values of the transient parameters could be gained by a coupling calculation in the steady-state. The transient rotating speed of the pump can be obtained computationally by UDF (user-defined functions) in Fluent software.

Speed transient law of rotating parts of pump unit

The change rule of rotating speed must be determined for the 1D-3D coupling calculation during power-supply failure because the transient parameters such as pressure, moment and flow velocity in a centrifugal pump system are closely related to the rotating speed change of the pump unit. In this section, the transient trends of pump parameters are obtained by the motion equation and resistance moment of pump unit during the power-supply failure.

The working state of the unit is determined by the algebraic summation of the driving moment M_P and resisting moment M_F, namely:

$$M = M_P - M_F = J\frac{d\omega}{dt} \tag{13}$$

where M is the moment of the pump rotating parts; M_P is the driving moment; M_F is the resisting moment including the resistance moment of fluid and the loss moment of the unit; $J = GD_R^2/(4g)$ is the inertia moment of the rotating parts; G is the weight of the rotating parts; D_R is the distance from the center of mass of the rotating parts to the rotating axle; and ω is the angular velocity.

When the pump-pipe system is powered off, the moment is only the resistance moment. M is only the resistance moment of fluid and the mechanical friction resistance moment caused by the bearing parts as the motor is not connective with the power grid. So Equation (13) is simplified as follows:

$$M = M_F = -J\frac{d\omega}{dt} \tag{14}$$

The transient trend of the rotating speed can be obtained by the integrating Equation (14) over the time when the resistance moment is provided.

CASE STUDIES AND ANALYSES

The numerical simulation of power-supply failure process for a pump-pipe hydraulic system of a double suction centrifugal pump based on the 1D-3D coupling method is carried out in this paper, and the calculated results are compared with experimental data and calculated results by 1D-MOC. The schematic layout of the pipeline is given in Figure 2. The basic characteristics of the pump unit are given above under 'Centrifugal pump-pipe hydraulic system' and '3D calculation schemes'. The initial flow rate before power-supply failure is 120 m^3/h and the initial rotating speed is 2,950 r/min. The transient process of power-supply failure of the centrifugal pump-pipe system is investigated systematically. The transient rotating speed is obtained by replacing the initial values into Equation (14).

The experimental system concerning the centrifugal pump-pipe (Zhu 2015) consists of a cavitation tank, pump, torque meter, converter motor, flow regulating valve, surge tank, valves and flowmeter as shown in Figure 7. The inlet diameter of the model pump is 100 mm, its outlet diameter is 80 mm, the rated flow rate is 80 m^3/h, the rated head is 15 m, the rated rotating speed is 2,950 r/min and the specific speed is $n_s = 3.65n\sqrt{Q/2}H^{3/4} = 148.91$. The pressures at the inlet and the outlet of pump are obtained by the piezoresistive pressure sensors, both of their measuring accuracies are 0.25% and their dynamic response times are less than 1 ms. The rotating speed and the power are obtained by the speed and torque dynamometer installed between the pump and the motor, its measuring accuracy is 0.18% FS and the sampling time interval is 1 ms in the experiment. The corresponding pressure difference between the inlet and the outlet of the pump is obtained (Zhu 2015).

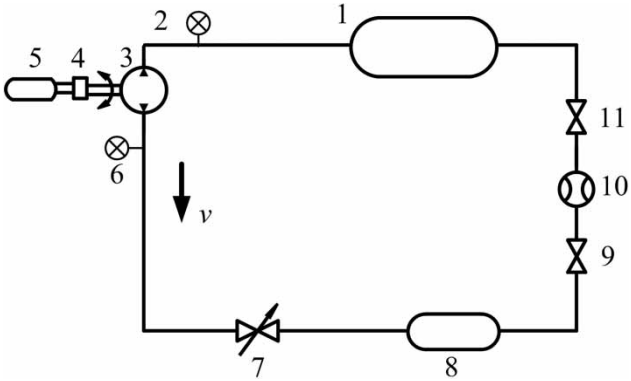

Figure 7 | Schematic layout of pump-pipe experimental system (Zhu 2015). 1. Cavitation tank; 2. Pressure gauge; 3. Pump; 4. Torque meter; 5. Converter motor; 6. Pressure gauge; 7. Flow regulating valve; 8. Surge tank; 9. Valve; 10. Flowmeter; 11. Valve.

Transient external characteristics of pump unit

The MOC is employed to solve Equations (1) and (2) along the characteristic line, where the central difference scheme is used for the flow rate term and the pressure term and the rectangular integration method is adopted for the rotating speed. The upstream reservoir is calculated by C− equation and the downstream reservoir is solved by C+ equation because the water levels are constants in upstream and downstream reservoirs. Based on Equations (6) and (7), the internal flow of the pump is calculated using Fluent software.

Figure 8 shows the transient process of the rotating speed and the flow rate predicted by 1D-MOC during the power-supply failure process, in which the dashed line is the rotating speed, the dotted line is the flow rate and the solid line is the experimental rotating speed. Figure 9 indicates the transient trends of the rotating speed and the flow rate calculated by the 1D-3D coupling method, in which the dashed line is the rotating speed, the dotted line is the flow rate and the solid line is the experimental rotating speed. At the beginning stage (0–3 s), the rotating speed decreases rapidly because the input power is zero, and the hydraulic resistance increases because of the pressure difference at the inlet and outlet of the pump, which leads to the

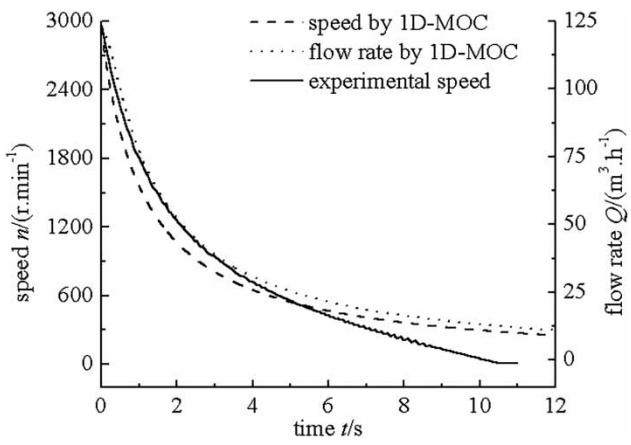

Figure 8 | Rotating speed and flow rate curves of 1D calculation.

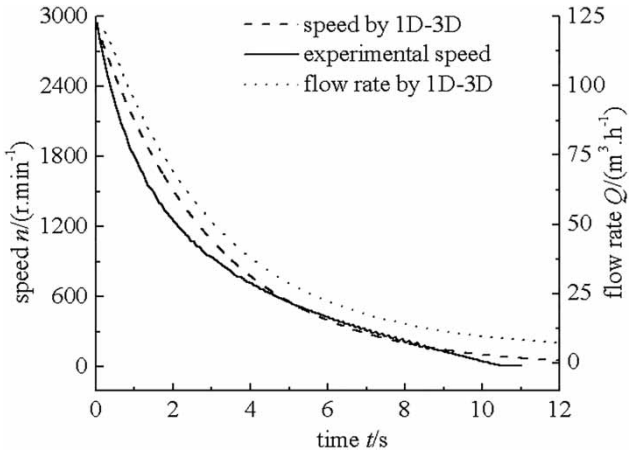

Figure 9 | Rotating speed and flow rate curves by coupling calculation.

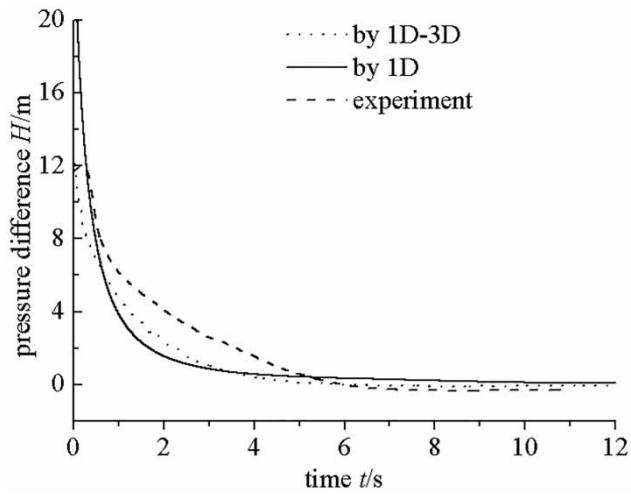

Figure 10 | Differential pressure curves of the pump.

rapid decrease in flow rate and the centrifugal effect of the flowing fluid in the impeller. Then, the rotating speed decreases slowly because of the slow decrease in the pressure difference at the inlet and outlet of the pump. The variation tendencies of rotating speeds predicted by 1D and 1D-3D methods are in accordance with the experimental data. However, the differences in rotating speeds between the 1D calculation and the experimental values are quite small at the beginning stage, and slightly larger at the stage after 8 s. Yet the accuracy of the coupling calculation is significantly higher than the 1D calculation values, especially after 6 s, the main reason for which may be that the steady friction is used instead of the unsteady friction, but the unsteady friction has a great influence on the phase of calculation results in the later stage of the transient process.

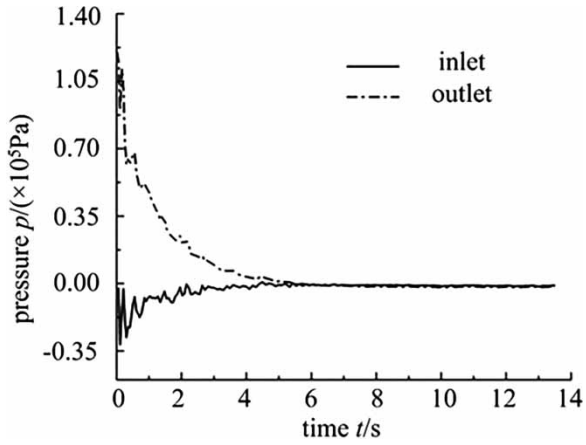

Figure 11 | Pressure curves at the inlet and outlet of the pump.

Figure 10 shows the three transient curves of pressure difference between the inlet and outlet of the pump during the power-supply failure process. The dashed line is obtained by experiment, the solid line is obtained by 1D-MOC, and the short dot line is obtained by the 1D-3D coupling method in which the rotating speeds are given by the motion equation of the pump rotating parts. The errors of the pressure differences obtained by the coupling calculation are smaller than those obtained by 1D-MOC, which indicates that the 1D-3D method can improve the calculated accuracy. Figure 11 shows the pressure traces at the inlet and outlet of the pump obtained by the 1D-3D coupling numerical method. The fluctuation is obvious during the power-supply failure process because of the change in flow rate. At the beginning stage (0–1 s), the pump outlet pressure reduces rapidly while the inlet pressure fluctuation is large because the input power reduces rapidly to zero, which leads to the most dramatic reduction in the pump head at this stage. At the middle stage (1–4 s), the pressure firstly fluctuates severely and then gradually changes to be synchronous because the fluctuating pressures at the inlet and the outlet caused by the transient flow are transmitted back and forth in the pipeline. After that, with the decreasing of the water hammer fluctuation, the pressure change becomes smooth because the interference between the static and dynamic interfaces reduces with the decreasing

flow rate and rotating speed. Finally, the pressures at the inlet and the outlet tend to be uniform.

Figure 12 shows the errors of the rotating speeds. The average computational errors of the rotating speeds obtained by the 1D-MOC method and by the 1D-3D coupling method are 151.938 and 89.176 r/min, respectively, and the corresponding root mean square errors (RMSEs) are 5.476 and 4.152 r/min, respectively. Figure 13 shows the difference between the calculated flow rate obtained by the 1D-3D method and that obtained by the 1D method. It can be seen from Figure 12 that when $t < 1.5$ s, the rotating speed obtained by the 1D-3D method increases with time while that by the 1D method decreases, so the difference between the water head calculated by the two methods increases with time, therefore, the flow difference calculated by the two methods increases with time. The trends of the calculated data obtained by the two methods are opposite to each other and intercross at the time of 5 s, and the difference between the flow rate calculated by the two methods decreases with time to the constant. The average computational error is 6.298 m^3/h and the RMSE is 0.267 m^3/h. Figure 14 shows the pressure difference predicted by the 1D-MOC and the 1D-3D at the inlet and the outlet of the pump. The dotted line is obtained by the 1D-3D method. Compared to the experimental data, the average computational errors of pressure difference obtained by the 1D-3D coupling calculated method and by the 1D-MOC calculation are 0.75 and 1.04 mH_2O, respectively, and the corresponding RMSEs are 1.05 and 1.66 mH_2O, respectively. According to Figure 13, the error of rotating speed between the calculated results by the 1D-3D method and the experimental data increases at first and then decreases, and the corresponding increase in the predicted rotating speed causes the increase in flow rate at first and then it decreases during simulation. According to the external characteristics of the centrifugal pump (Zhu 2015), with the increase of flow rate, the pressure difference at the inlet and the outlet decreases. Therefore, the pressure difference at the inlet and the outlet of the pump decreases at first, and then increases. The comparisons show that all the

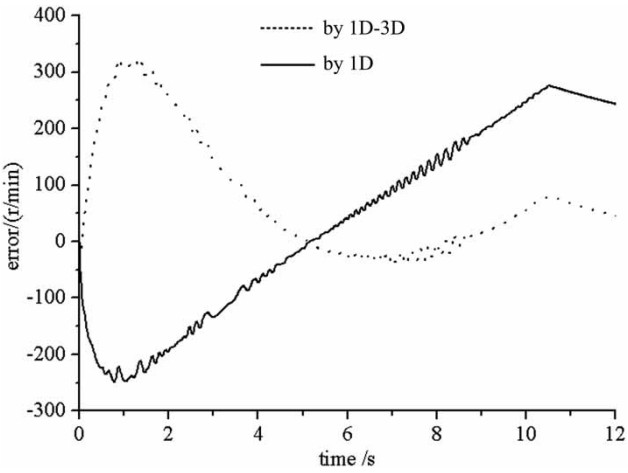

Figure 12 | Error of rotating speed between calculated and experimental data.

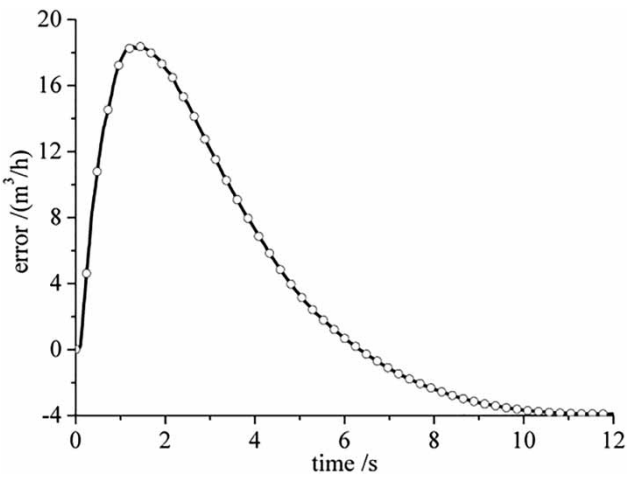

Figure 13 | Difference of flow rate obtained by the 1D-3D and 1D methods.

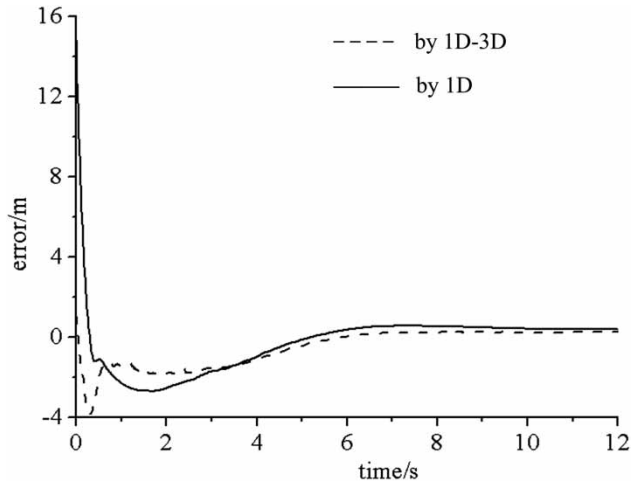

Figure 14 | Pressure difference predicted by the 1D-MOC and 1D-3D methods at the inlet and outlet of pump.

average errors are closer to the experimental values than the RMSE values, and the computational results by the 1D-3D coupling method are closer to the experimental values than those by the 1D method.

Transient internal characteristics of pump

Figure 15 shows the pressure change on the central cross-section of a single impeller during the power-supply failure process. With the decrease of the rotating speed, the pump pressure gradient changes significantly. At the beginning of the transient stage the area of the negative pressure in the impeller is larger, and then the flow rate decreases and the pump inlet pressure increases, which causes the total pressure of the pump to increase. At the same time, the output work of the pump decreases and the pump outlet pressure reduces, the water hammer wave travels back and forth in the pump. Then, the negative pressure zone gradually disappears, which indicates that the water hammer wave weakens due to the frictional resistance. After 10 s, the transient process ends, the impeller output power is close to zero, the flow rate in the pump is very low, and the pressures at the pump inlet and outlet are close to zero.

Figure 16 shows the streamline evolution diagram in the volute region in the power-supply failure process. At the early stage of the transient process, the flow inside the impeller is smooth, and the streamline is even from the impeller to the volute. After 1.48 s, the streamline begins to be uneven gradually at off-design conditions of flow rate and gradually deviates from those at the rated flow rate. As the flow rate decreases, the streamline becomes confused, and the influence of the volute tongue on the flow becomes more and more significant. When the flow rate is very small ($Q = 0.08Q_r$), many vortexes fill in the volute and the flow channel is almost blocked.

Figure 17 shows the pressure evolution diagram on a cylindrical section between the volute and impeller with a radius of 68 mm, in which the front cover and the back cover are also labeled. At the early stage of pump stopping ($t = 0.008$–0.68 s), the pressure on the cylinder surface fluctuates greatly due to the water hammer. Furthermore, there is always an obvious low pressure area near the tongue of the cylinder section. The low pressure area may be caused by the dynamic and static interference between the volute tongue and the impeller. With the decrease of the rotating speed, the pressure in the high pressure area decreases gradually, while the pressure in the low pressure area increases gradually until the pressures are all zero because the dynamic and static interference between the tongue and the impeller gradually weaken.

Influence of coupling parameters

The convergence of the physical quantities on the 1D-3D coupling interface should be taken into account in the coupling calculation method. The parameters that affect the coupling convergence and stability mainly include the coupling relaxation factor and the number of iterations of the CFD in each time step.

Coupling relaxation factor

In the data transfer between the lD-MOC and 3D CFD method, the transferred coupling parameter q for the ith times is as follows:

$$q_1^{t_1+1} = (1-\delta)q_1^{t_1} + \delta q_2^{t_1+1} \tag{15}$$

where δ is the coupling relaxation factor; subscripts 1 and 2 are the transfer and receiver of the coupling of physical quantities, respectively; superscript t_1 is the coupling moment.

The relaxation factor affects the convergence rate and stability of the coupling. The calculated pressure difference between the inlet and the outlet of pump has a relationship with different coupling relaxation factors as shown in Figure 18. At the beginning stage (0–1 s) of the transient process, when the relaxation factor is small, the calculated fluctuation of pressure difference is obvious and the convergence rate is slow, which can lead to large computation errors. With the increasing of the relaxation factor, the fluctuation of coupling calculation is gradually weakened. If the relaxation factor is too large, it may lead to computational instability. For example, when δ is increased to 0.8, there is fluctuation in the later stage. Therefore, the convergence rate and the coupling stability should be considered synthetically. It is suitable when the value of δ is 0.4 in this case.

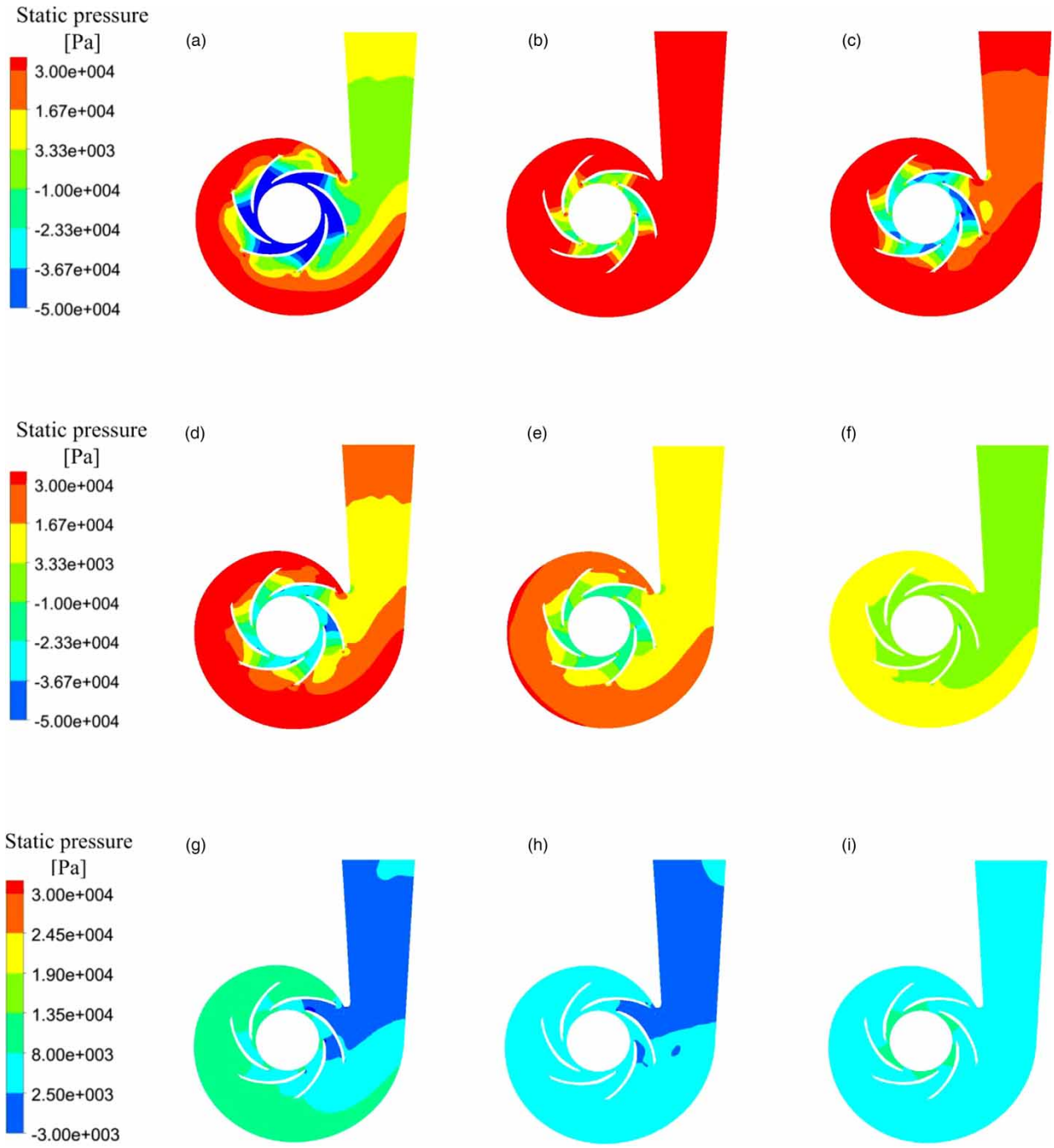

Figure 15 | Pressure change on the center cross-section of a single impeller during power-supply failure. (a) $t = 0.008$ s, $Q = 1.51Q_r$, (b) $t = 0.04$ s, $Q = 1.48Q_r$, (c) $t = 0.28$ s, $Q = 1.38Q_r$, (d) $t = 0.68$ s, $Q = 1.21Q_r$, (e) $t = 1.48$ s, $Q = 0.94Q_r$, (f) $t = 3.5$ s, $Q = 0.51Q_r$, (g) $t = 7$ s, $Q = 0.21Q_r$, (h) $t = 10$ s, $Q = 0.12Q_r$, (i) $t = 13$ s, $Q = 0.08Q_r$.

Number of iterations in each time step

The number of iterations of each time step in CFD not only affects the coupling convergence in each time step but also the rate of the coupling calculation and the calculation accuracy. If the number of iterations is too small, it is difficult to obtain convergence and stability of the coupling transfer parameters. If the number of iterations is too large, although

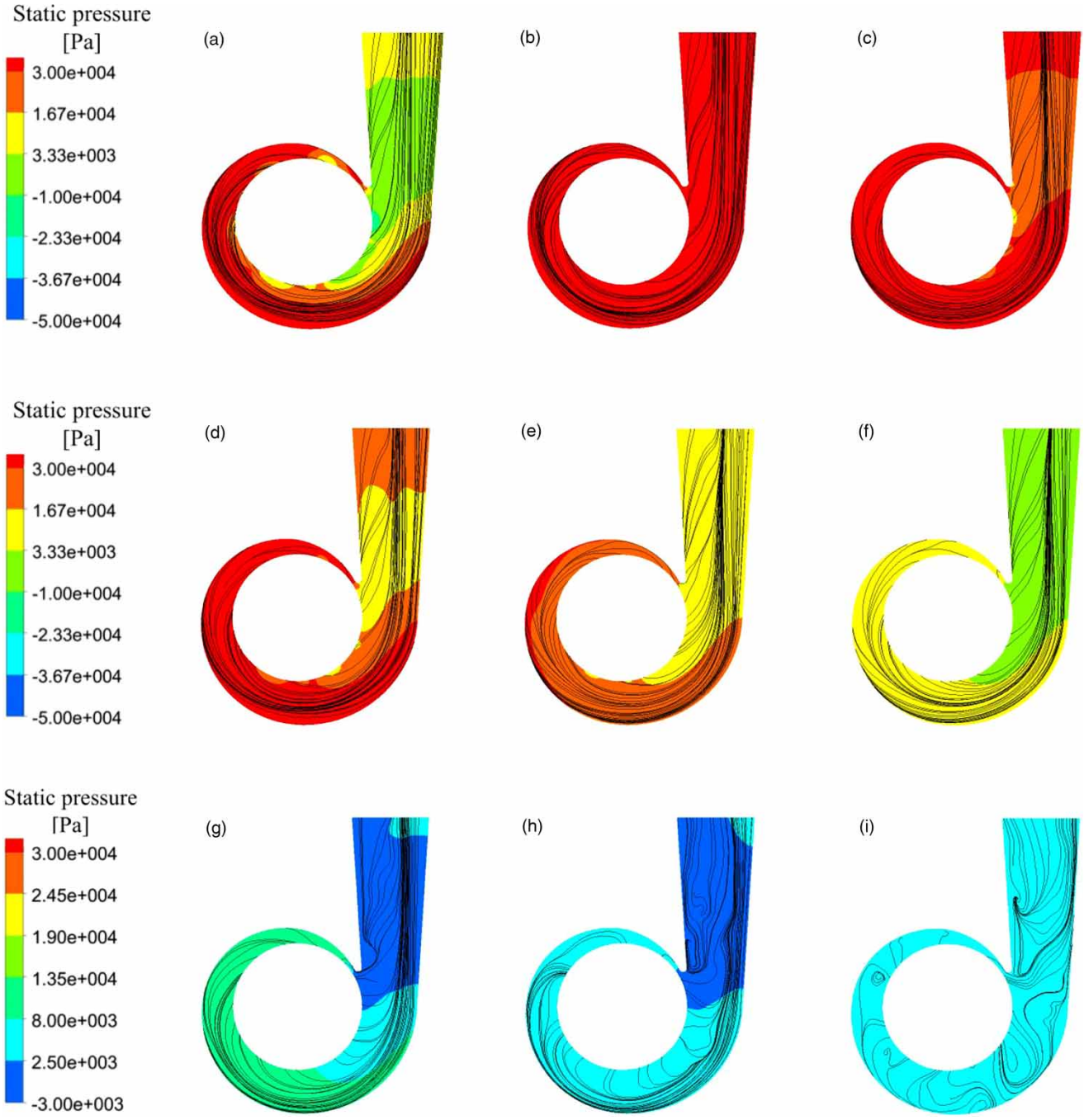

Figure 16 | Streamline evolution diagram of the volute region in the power-supply failure process. (a) $t = 0.008$ s, $Q = 1.51Q_r$, (b) $t = 0.04$ s, $Q = 1.48Q_r$, (c) t = 0.28 s, $Q = 1.38Q_r$, (d) $t = 0.68$ s, $Q = 1.21Q_r$, (e) $t = 1.48$ s, $Q = 0.94Q_r$, (f) $t = 3.5$ s, $Q = 0.51Q_r$, (g) $t = 7$ s, $Q = 0.21Q_r$, (h) $t = 10$ s, $Q = 0.12Q_r$, (i) $t = 13$ s, $Q = 0.08Q_r$.

the convergence of the coupling parameters can be guaranteed, the calculation time will be increased, and coupling efficiency will be influenced. Therefore, in order to obtain accurate calculation results, a reasonable iteration number in each time step in CFD should be adopted. The iteration numbers including 50, 100, 200, 300, 400, and 500 times are selected for calculating, respectively. Figure 19 shows the influence of iteration numbers in each time step on the

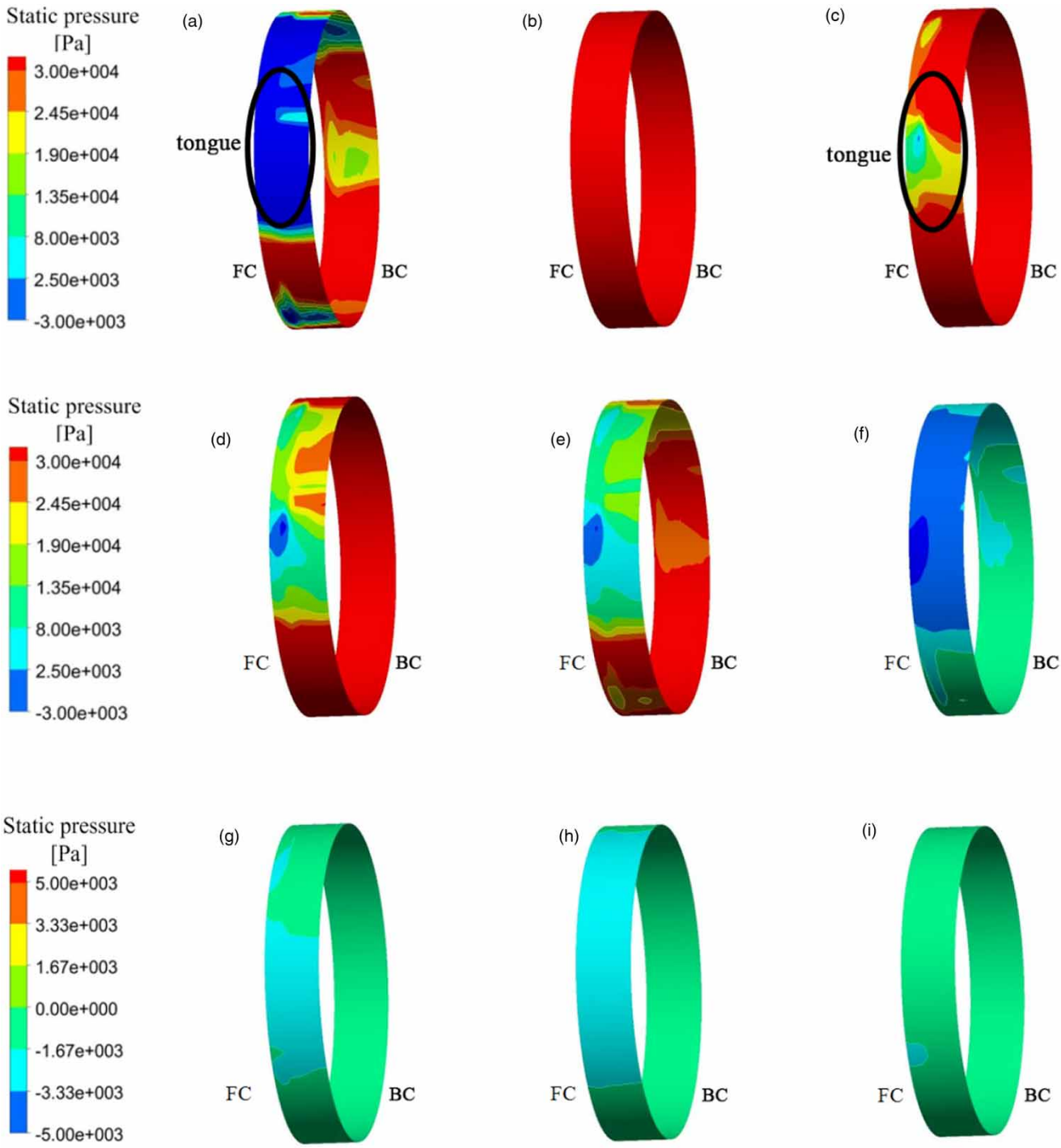

Figure 17 | Pressure on the cylinder section in conditions of power-supply failure. (a) $t = 0.008$ s, $Q = 1.51$Qr, (b) $t = 0.04$ s, $Q = 1.48$Qr, (c) $t = 0.28$ s, $Q = 1.38$Qr, (d) $t = 0.68$ s, $Q = 1.21$Qr, (e) $t = 1.48$ s, $Q = 0.94$Qr, (f) $t = 3.5$ s, $Q = 0.51$Qr, (g) $t = 7$ s, $Q = 0.21$Qr, (h) $t = 10$ s, $Q = 0.12$Qr, (i) $t = 13$ s, $Q = 0.08$Qr.

pressure difference between the inlet and the outlet. When the iteration number is 50, the coupling calculation convergence fluctuates widely, and the coupling calculation is very unstable. With the number of iterations increasing, the coupling stability is increased. When the iteration number is more than 300, the speed of curve convergence is fast

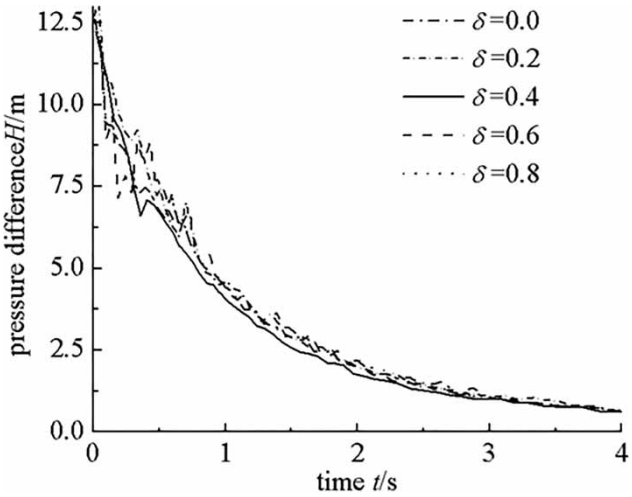

Figure 18 | Influence of coupling relaxation factor on pressure difference.

and the increase of the iteration number does not affect the coupling stability, but increases the coupling calculation time. Therefore, considering the computational efficiency and the coupling convergence, the suitable iterative step for each time step of CFD is selected for 300 times in this case.

Influence of coupling solution mode

The coupling method will affect the calculated results. In view of the characteristics of the pipe system, three schemes of synchronous serial coupling (SSC), synchronous parallel coupling (SPC) and asynchronous serial coupling (ASC) are employed to analyze the turbulent flows inside the centrifugal pump and to obtain the performance parameters of the pump-pipe system. Three schemes are shown in Figure 20, in which code A and code B represent Flowmaster and Fluent, respectively. SSC and SPC use different algorithms, and data exchanges are carried out on each time node at the same moment. Based on the SSC, the data is passed from Fluent to Flowmaster at first, and then the Flowmaster finishes the computation and the new data obtained from the Flowmaster is passed to Fluent for the next step calculation; all the processes of all transferred data are a one-way scheme. Based on the SPC, the data is passed from Fluent to Flowmaster at first (one-way data-passing scheme), and when the Flowmaster receives the transferred data, both the Flowmaster and the Fluent synchronously finish the computation at the same time step (synchronous parallel computation), and then both exchange the new data with each other (two-way data-passing scheme), and begin to carry out the next step calculation. Based on the ASC, after the Fluent performing 3D CFD for integer multiple time steps of 1D-MOC, the Flowmaster begins to perform 1D-MOC, and the data is passed from Fluent to Flowmaster at first, and then the Flowmaster finishes the computation for integer multiples. The new data obtained from the Flowmaster is passed to the Fluent for the next step calculation and all the processes of all transferred data are a one-way scheme. In order to ensure that those two software output data at the same time, the time step in Fluent software should be an integral multiple of this in Flowmaster software.

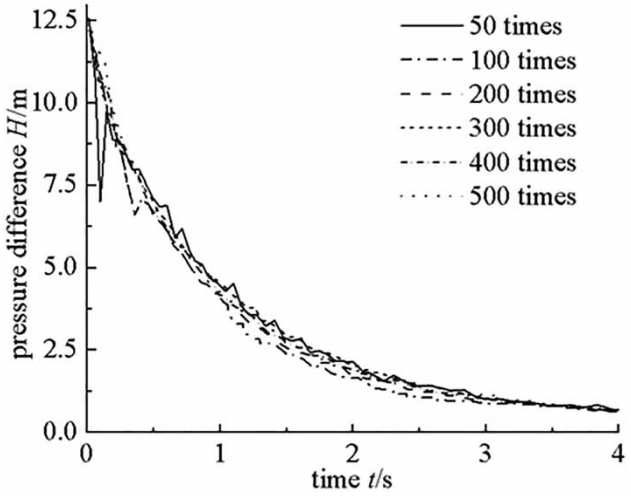

Figure 19 | Influence of number of iteration in each time step on pressure difference.

Influence of coupling solution mode on transient performance

The pressure difference at the inlet and the outlet of the pump and the flow rate are obtained by the above three schemes, respectively, as shown in Figure 21. The solid data is from the ASC, the dash data is from the SSC and the dot data is from the SPC. The computational results obtained by the SSC and the SPC are close to each other, and the calculated results obtained by the ASC are slightly different from those by the SSC and the SPC due to the different coupling mode.

The data transmission errors from the SSC and the SPC are smaller than those from the ASC based on MpCCI,

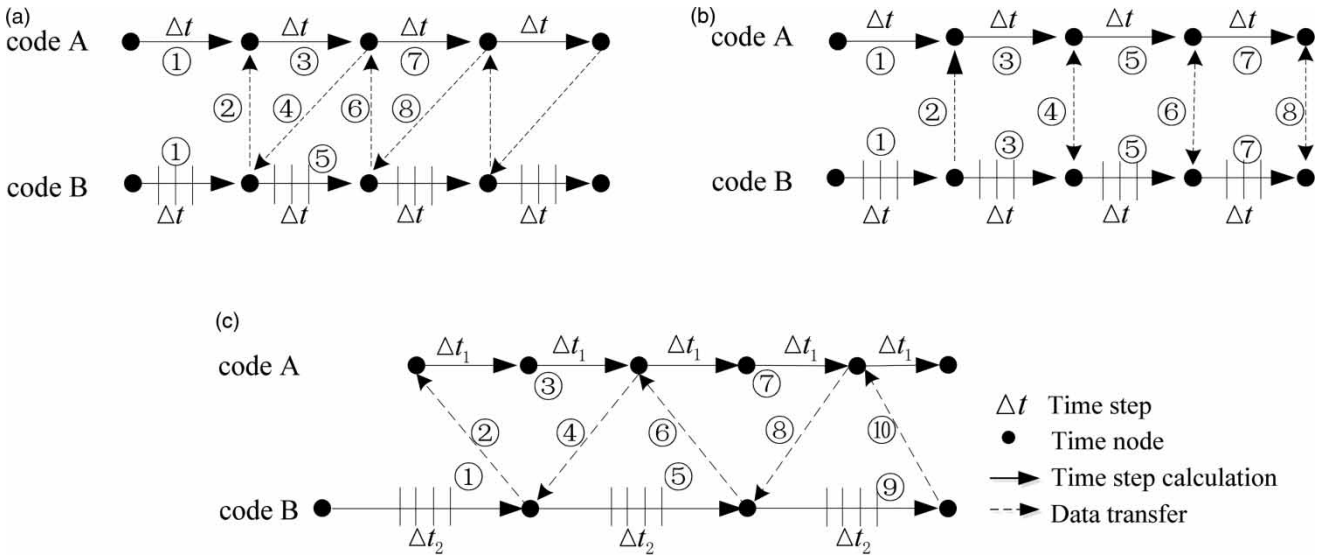

Figure 20 | Three coupling solution modes. (a) Synchronous serial coupling mode (SSC), (b) synchronous parallel coupling mode (SPC), (c) asynchronous serial coupling method (ASC).

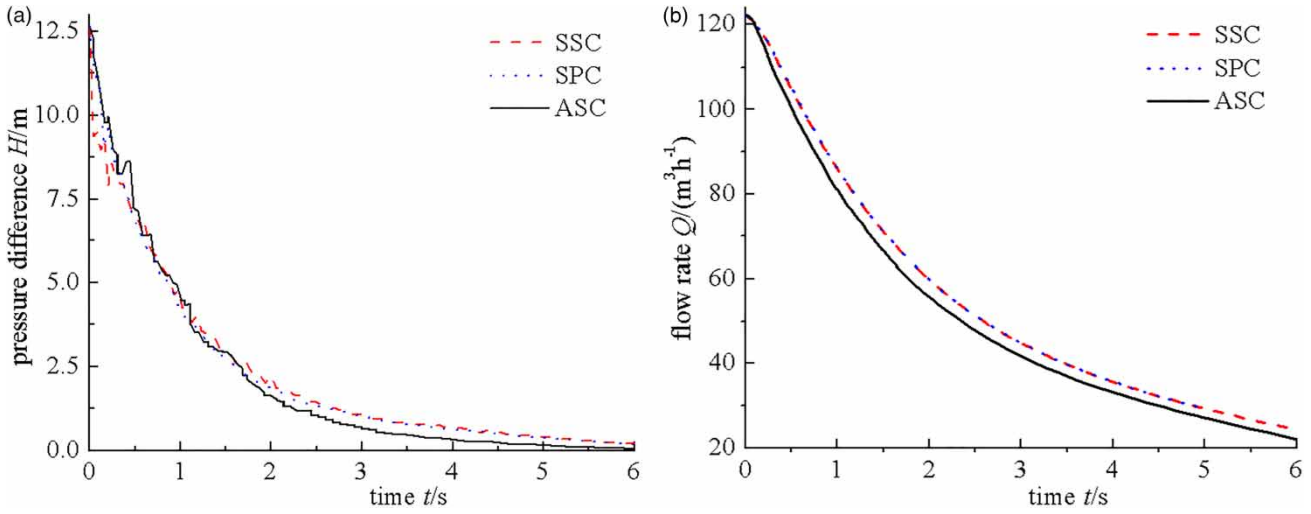

Figure 21 | Pressure difference and flow rates by three coupling solution methods. (a) Pressure difference against time, (b) flow rate against time.

because 1D and 3D are performed independently using their own codes and are called through the coupling server processes, and data may be lost during the data exchange, especially for the asynchronous couple. The data is not transmitted in time. The computed results obtained by the SSC and the SPC modes are relatively close because both of them are synchronous coupling solution modes. However, the precision predicted by the SPC is less than that by the SSC, and the fluctuation of pressure difference by the SSC is more obvious than that by the SPC, and the stability of the calculation is relatively poor. The new data passed by Fluent is used for 1D-MOC calculation in Flowmaster while the old data on the previous time step is still used to calculate in Fluent from the second time step by the SPC mode, which results in the accumulated error caused by time lag.

A monitoring point is set on the blade to obtain the transient pressure, the location of the monitoring point is shown in Figure 22(a) and the rules of transient pressure change are shown in Figure 22(b). The pressure fluctuations

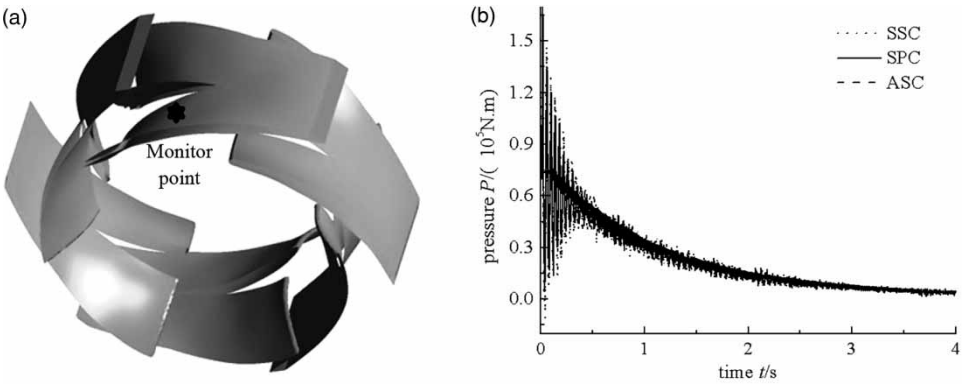

Figure 22 | Position of monitoring point on the blade and pressure change. (a) Position of pressure monitoring point on blade, (b) pressure on monitoring point of blade.

on the blade obtained by the SPC and the SSC are relatively large, which is more consistent with the characteristics of the transient process of power-supply failure. The pressure fluctuations calculated by the ASC are relatively small, which is probably because the coupling method between Fluent and Flowmaster is asynchronous and the pressure wave is not transmitted in time.

Influence of coupling solution mode on internal flow in pump

The transient pressures at four moments, including $t_1 = 0.008$ s, $t_2 = 0.016$ s, $t_3 = 4$ s and $t_4 = 7.2$ s, are analyzed by using the three different coupling modes in order to explore the influence of the data transfer mode on the internal flow in pump. Figure 23 shows the static pressure distributions on the impeller symmetrical surface perpendicular to the axis at different times in the transient process. The internal flow laws obtained by the SSC and the SPC modes are similar to each other. They could all capture the transient wave process of the water hammer in the pump. The pressure inhomogeneity inside the impeller is obvious before moment t_2 due to the water hammer wave, but the pressure inhomogeneity range by the SSC is greater. The pressure change obtained by the ASC is relatively stable, and the pressure inhomogeneity could not be captured. The flow in the impeller is gradually stable because of the gradual stability of the coupling calculation. The differences predicted by the three coupling solutions becomes less obvious, and the pressure distributions predicted by the three schemes tend to be consistent.

CONCLUSIONS

The transient calculations and analyses of the main dynamic parameters for the centrifugal pump-pipe hydraulic system in the power-supply failure process are carried out by using the 1D-3D coupling method and 1D-MOC, respectively. The 1D-3D results are compared to the experimental data and the results obtained by 1D-MOC. The main conclusions are as follows:

(1) In the power-supply failure process for the pump-pipe hydraulic system, the changing trends of rotating speed obtained by the 1D-3D coupling method and by the 1D-MOC are in agreement with the experimental data. All the average errors of transient parameters obtained by using the 1D-3D coupling method are closer to the experimental values than those by 1D-MOC, and the average errors RMSE by the 1D-3D coupling method are closer to the experimental values than those by 1D-MOC. At the beginning stage of the power-supply failure process, the pressure gradient in the pump changes significantly and the area of negative pressure in the impeller is larger. With the decrease of rotating speed, the flow rate decreases and the negative pressure area disappears gradually to near zero. In addition, as the rotating speed and flow rate continues to decline, the flow velocity is also decreasing, and the effect of the volute tongue on streamline becomes more and more obvious.
(2) The data transmission errors of the pressure difference between the inlet and the outlet of the pump and the flow rate obtained by the SSC and the SPC are relatively

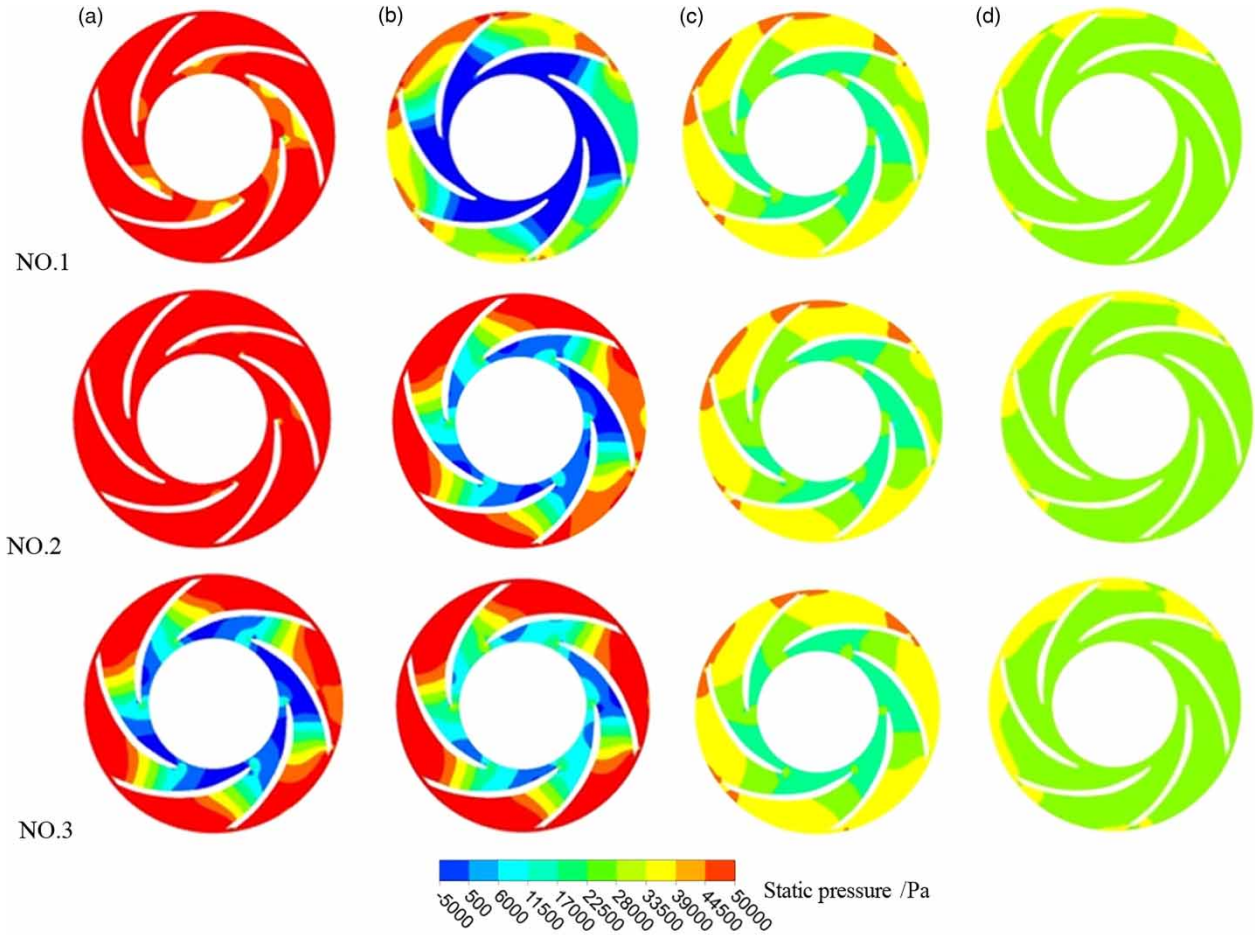

Figure 23 | Pressure cloud on the symmetrical surface of a single impeller at different times in the pump stopping process. (a) $t_1 = 0.008$ s, (b) $t_2 = 0.016$ s, (c) $t_3 = 4.0$ s, (d) $t_4 = 7.2$ s.

close to each other and are smaller than those from the ASC based on MpCCI. However, the precision predicted by the SPC is less than that by the SSC, and the internal flow laws obtained by these two modes could all capture the transient wave process of the water hammer in the pump while the pressure inhomogeneity obtained by the ASC could not be captured.

(3) With the increase of the relaxation factor, the fluctuation of coupling calculation gradually weakened. If the relaxation factor is too large, it may lead to computational instability. With the number of iterations increasing, the coupling stability increases, but when it is larger than a certain value, it does not affect the coupling stability, but increases the coupling calculation time.

The above analyses and comparisons indicate that the proposed 1D-3D coupling method and numerical techniques are reliable in predicting the power-supply failure process for a pump-pipe system with a complex structure, and are also applicable to the transient research of hydraulic systems with hydraulic machinery.

ACKNOWLEDGEMENTS

This work was supported by the National Natural Science Foundation of China (Grant Nos. 51779257, 51479196).

REFERENCES

Acosta, S., Puelz, C., Rivière, B., Penny, D. J. & Rusin, C. G. 2015 Numerical method of characteristics for one-dimensional blood flow. *J. Comput. Phys.* **294** (C), 96–109.

Chaudhry, H. M. 2014 *Applied Hydraulic Transients*. Springer-Verlag, New York.

Cui, B. L., Lin, Z., Zhu, Z. C., Wang, H. & Ma, G. 2017 Influence of opening and closing process of ball valve on external performance and internal flow characteristics. *Exp. Thermal Fluid Sci.* **80**, 193–202.

Freni, G., Marchis, M. D. & Napoli, E. 2013 Implementation of pressure reduction valves in a dynamic water distribution numerical model to control the inequality in water supply. *J. Hydroinform.* **16** (1), 207–217.

Grunloh, T. P. & Manera, A. 2016 A novel domain overlapping strategy for the multiscale coupling of CFD with 1D system codes with applications to transient flows. *Ann. Nucl. Energy* **90**, 422–432.

Hooff, T. V., Blocken, B. & Tominaga, Y. 2017 On the accuracy of CFD simulations of cross-ventilation flows for a generic isolated building: comparison of RANS, LES and experiments. *Build. Environ.* **114**, 148–165.

Hwang, Y. H., Huang, H. S., Chung, N. M. & Wang, P. Y. 2012 Particle method of characteristics (PMOC) for unsteady pipe flow. *J. Hydroinform.* **15** (3), 780–797.

Kiyama, A., Tagawa, Y., Ando, K. & Kameda, M. 2016 Effects of a water hammer and cavitation on jet formation in a test tube. *J. Fluid Mech.* **787** (2), 224–236.

Kong, F., Kim, H. D., Setoguchi, T. & Kim, J. 2015 Starting transient flows in a chevron ejector-diffuser system. *J. Mech. Sci. Technol.* **29** (3), 887–892.

Koufi, L., Younsi, Z., Cherif, Y. & Naji, H. 2017 Numerical investigation of turbulent mixed convection in an open cavity: effect of inlet and outlet openings. *Int. J. Therm. Sci.* **116**, 103–117.

Liu, J., Liu, S., Sun, Y., Jiao, L., Wu, Y. & Wang, L. 2013 Three-dimensional flow simulation of transient power interruption process of a prototype pump-turbine at pump mode. *J. Mech. Sci. Technol.* **27** (5), 1305–1312.

Martins, N. M. C., Soares, A. K., Ramos, H. M., Ramos, H. M. & Covas, D. I. C. 2016 CFD modeling of transient flow in pressurized pipes. *Comput. Fluids* **126** (1), 129–140.

Martins, N. M. C., Brunone, B., Meniconi, S., Ramos, H. M. & Covas, D. I. C. 2017 CFD and 1D Approaches for the unsteady friction analysis of low Reynolds number turbulent flows. *J. Hydr. Eng.* **143** (12), 04017050.

Martins, N. C., Brunone, B., Meniconi, S., Ramos, H. M. & Covas, D. I. C. 2018 Efficient CFD model for transient laminar flow modeling: pressure wave propagation and velocity profile changes. *J. Fluids Eng. ASME* **140** (1), 011102.

Meniconi, S., Duan, H. F., Brunone, B., Lee, P. J., Ghidaoui, M. S. & Ferrante, M. 2014 Further developments in rapidly decelerating turbulent pipe flow modeling. *J. Hydr. Eng.* **140** (7), 04014028.

Nerella, R. & Rathnam, E. V. 2015 Fluid transients and wave propagation in pressurized conduits due to valve closure. *Proc. Eng.* **127**, 1158–1164.

Panov, L. V., Chirkov, D. V., Cherny, S. G. & Pylev, I. M. 2014 Numerical simulation of pulsation processes in hydraulic turbine based on 3D cavitating flow. *Thermophys. Aeromech.* **21** (1), 31–43.

Pei, J., Yuan, S. & Yuan, J. 2013 Fluid-structure coupling effects on periodically transient flow of a single-blade sewage centrifugal pump. *J. Mech. Sci. Technol.* **27** (7), 2015–2023.

Wang, C. & Yang, J. D. 2015 Water hammer simulation using explicit–implicit coupling methods. *J. Hydr. Eng.* **141** (4), 04014086.

Wang, C., Nilsson, H., Yang, J. & Petit, O. 2017 1D-3D coupling for hydraulic system transient simulations. *Comput. Phys. Commun.* **210**, 1–9.

Watanabe, N., Kubo, M. & Yomoda, N. 2006 An 1D-3D integrating numerical simulation for engine cooling problem. *Dublin Inst. Technol.* **64** (5), 438–443.

Wylie, E. B. & Streeter, V. L. 1993 *Fluid Transient in Systems*. Prentice-Hall, Englewood Cliffs, New Jersey, USA.

Zhang, X. X., Cheng, Y. G., Yang, J. D., Xia, L. S. & Lai, X. 2014 Simulation of the load rejection transient process of a francis turbine by using a 1-D-3-D coupling approach. *J. Hydrodynam.* **26** (5), 715–724.

Zhao, W. & Zhao, G. 2018 Numerical investigation on the transient characteristics of sediment-laden two-phase flow in a centrifugal pump. *J. Mech. Sci. Technol.* **32** (1), 167–176.

Zhou, B., Yuan, J., Lu, J., Sun, W., Yin, L. & Ji, P. 2017 Investigation on transient behavior of residual heat removal pumps in 1000 MW nuclear power plant using a 1D-3D coupling methodology during start-up period. *Ann. Nucl. Energy.* **110**, 560–569.

Zhu, Q. 2015 *Study on Transient Characteristics of Double-Suction Centrifugal Pump System in Startup Processes*. China Agricultural University, Beijing.

Zou, Z. C., Wang, F. J., Yao, Z. F., Tao, R., Xiao, R. F. & Li, H. C. 2016 Impeller radial force evolution in a large double-suction centrifugal pump during startup at the shut-off condition. *Nucl. Eng. Des.* **310**, 410–417.

First received 6 November 2018; accepted in revised form 3 June 2019. Available online 22 July 2019